ACS APPLIED MATERIALS & INTERFACES

www.acsami.org

Research Article

Shape-Controlled and Well-Arrayed Heterogeneous Nanostructures via Melting Point Modulation at the Nanoscale

Zhi-Jun Zhao, Junseong Ahn, Jiwoo Ko, Yongrok Jeong, Moonjeong Bok, Soon Hyoung Hwang, Hyeok-Joong Kang, Sohee Jeon, Jungrak Choi, Inkyu Park,* and Jun-Ho Jeong*

Cite This: *ACS Appl. Mater. Interfaces* 2021, 13, 3358−3368

Read Online

ACCESS | Metrics & More | Article Recommendations | Supporting Information

ABSTRACT: A novel method for fabricating shape-controlled and well-arrayed heterogeneous nanostructures by altering the melting point of the metal thin film at the nanoscale is proposed. Silver nanofilms (AgNFs) are transformed into silver nanoislands (AgNIs), silver nanoparticles (AgNPs), and silver nanogaps (AgNGs) that are well-ordered and repositioned inside the gold nanoholes (AuNHs) depending on the diameter of the AuNHs, the thickness of the AgNF, and the heating temperature (120−200 °C). This method demonstrates the ability to fabricate uniform, stable, and unique structures with a fast, simple, and mass-producible process. For demonstrating the diverse applicability of the developed structures, high-density AgNGs inside the AuNHs are utilized as surface-enhanced Raman spectroscopy (SERS) substrates. These AgNGs-based SERS substrates exhibit a performance enhancement, which is 1.06×10^6 times greater than that of a metal film, with a relative standard deviation of 19.8%. The developed AgNP/AgNI structures are also used as nonreproducible anti-counterfeiting signs, and the anti-counterfeiting/readout system is demonstrated via image processing. Therefore, our method could play a vital role in the nanofabrication of high-demand nanostructures.

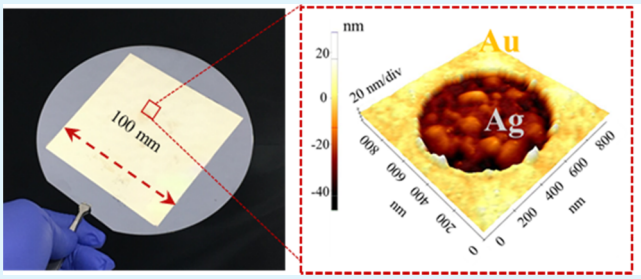

KEYWORDS: *heterogeneous nanostructures, silver nanoparticles (Ag NPs), metal nanogaps, surface-enhanced Raman spectroscopy (SERS), anti-counterfeiting*

Downloaded via KOREA ADVANCED INST SCI AND TECHLGY on March 2, 2021 at 07:53:30 (UTC).
See https://pubs.acs.org/sharingguidelines for options on how to legitimately share published articles.

INTRODUCTION

Heterogeneous nanostructures, unique nanoarchitecture with bi- or multimetallic construction, have gained considerable attention in the development of catalysts,[1,2] sensors,[3−5] transistors,[6] nanogenerators,[7] photovoltaic devices,[8] batteries,[9] metasurfaces,[10,11] and plasmonic structures.[12,13] In these devices, the core elements with unprecedented performance are nano-manufactured functional materials, such as nanoparticles, nanorods, nanowires, nanopillars, nanoboxes, and nanoribbons, whose physical properties and functions are fundamentally different from those of the bulk materials.[14,15] In particular, the combination of unique nanostructures and multiple noble metal construction provides enhanced catalytic properties and optical properties. For example, several studies have reported reliable and sensitive gas sensors based on heterogeneous nanowires with various noble-metal (e.g., Ag, Au) catalysts.[16−18] Additionally, various other noble metal-based heterogeneous nanostructures with ultra-small nanogaps (including nanoparticles, nanopillars, nanoboxes) have been extensively fabricated. Successful fabrication and application of these nanostructures have also been reported in surface-enhanced Raman spectroscopy (SERS), largely because of the plasmonic effect of Ag and Au at the nanoscale.[19−21] Also, the heterogeneous nanostructures are widely used in the field of anti-counterfeiting signs since they have nonreproducible characteristics.[22,23] These heterogeneous nanostructures can be fabricated using conventional methods such as chemical synthesis,[24,25] physical evaporation,[26,27] electrospinning,[28] epitaxial growth,[29,30] focused ion beam,[31,32] and e-beam lithography.[33] Noble metals such as Ag, Au, and Pt can be used as catalysts for improving the device performance. Among these, the use of focused ion beam (FIB)-milling and e-beam lithography offer precise control of the geometry of these nanostructures. However, although these nanofabrication methods can produce well-arrayed heterogeneous nanostructures, they are expensive and time-consuming; consequently, these methods find limited applications in mass production. Other nanofabrication methods, such as spray coating and chemical synthesis, cannot easily achieve well-arrayed nanostructures. Furthermore, these methods require complex

Received: October 9, 2020
Accepted: December 11, 2020
Published: December 21, 2020

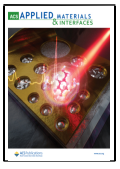

© 2020 American Chemical Society

https://dx.doi.org/10.1021/acsami.0c18122
ACS Appl. Mater. Interfaces 2021, 13, 3358−3368

posttreatment processes for their application in functional devices.

In an attempt to address the limitations outlined above, this study proposes a novel method for the fabrication of shape-controlled and well-arrayed heterogeneous nanostructures by adjusting the melting temperature of noble metals at the nanoscale. One of the findings of this study is that the geometry of the surrounding Au nanostructure plays a key role in the alignment and repositioning of the inner Ag nanostructures. The proposed method can control the shapes of the metal nanofilms (MNFs) from nanoislands to nanoparticles and nanogaps depending on the heating temperature, the thickness of the nanofilm, and the size of the nanostructure.

To demonstrate the utility and diverse applicability of the obtained nanostructures, SERS substrates and anti-counterfeit signs with various types of heterogeneous nanostructures were evaluated. The developed Ag−Au heterogeneous nanostructures were observed to exhibit ~10^6 times higher performance enhancement of the Rhodamine6G (R6G) Raman signal compared to that of a metal film. Furthermore, the nanostructures also provided reasonable uniformity with a relative standard deviation (RSD) within 19%. This superior performance can be attributed to the high density of the silver nanogaps (AgNGs) formed inside the uniformly arranged gold nanohole (AuNH) arrays. In addition, the nonreproducible nanostructures obtained using our proposed method were also demonstrated as anti-counterfeit signs on a polyimide (PI) film. By assigning a security code to each structure according to the number, average size, and fill ratio of the nanoislands, the heterogeneous nanostructure had a unique code that could not be mimicked, thereby confirming the effectiveness of the developed nanostructures as anti-counterfeit signs. Therefore, we believe that our method can bring innovations to various applications including biodetecting, gas sensing, and anti-counterfeiting fields.

RESULTS AND DISCUSSION

The morphology of the fabricated heterogeneous nanostructures was changed from the nanofilm to the nanoparticles, nanoislands, and nanogaps by controlling the heating temperature, the diameter of AuNHs, and the thickness of silver nanofilm (AgNF). To distinguish the shapes of the fabricated nanostructures clearly, Figure 1 shows three kinds of nanostructures that were developed in this study. The silver nanoparticle (AgNP) structure was defined as hemispherical shaped-Ag isolated inside the AuNHs, and the silver nanoisland (AgNI) structure was defined as an assembly of nanoscale Ag islands located inside the AuNHs, as shown in Figure 1(1) and (2), respectively. These structures are the results of the complete reshaping of the AgNF during the heating and cooling process. On the other hand, when only the surface of AgNF was partially melted, dense nanogaps were formed inside the AgNHs. This nanostructure with an extremely rough surface was named the AgNGs structure, as shown in Figure 1(3). All of these nanostructures can be fabricated by controlling the heating temperature, the diameter of AuNHs, and the thickness of AgNF that are directly related to the melting point of the metal at the nanoscale and the boundary constraints.

Figure 2 shows the fabrication process, large-area sample, and three-dimensional (3D) images of heterogeneous nanostructures. The polymer mold with the nanoholes can be

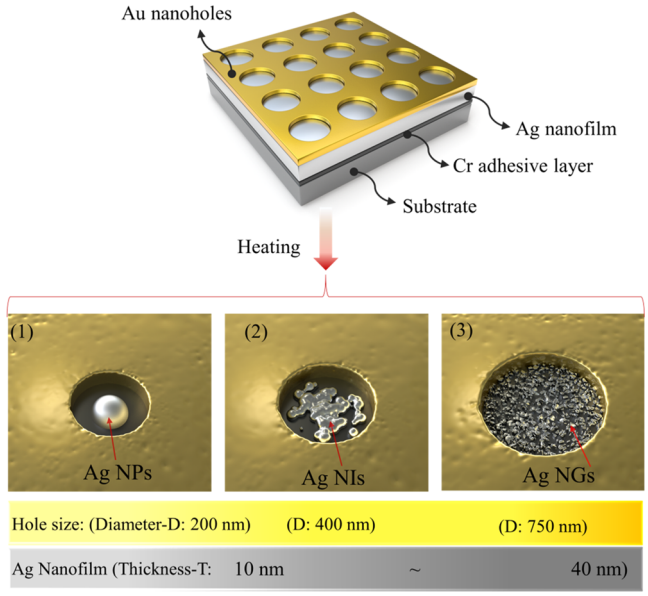

Figure 1. Schematic of the various shapes of the fabricated heterogeneous nanostructures depending on the heating temperature, diameter of AuNHs, and the thickness of AgNFs. (1) Ag nanoparticles (AgNPs) formed within AuNHs with a diameter of 200 nm. (2) Ag nanoislands (AgNIs) formed within AuNHs with a diameter of 400 nm. (3) Ag nanogaps (AgNGs) formed within AuNHs with a diameter of 750 nm.

repeatedly fabricated via the nanoimprint method (see Figure 2a(1−5)). (Detailed explanations are provided in the Methods section.) Then, gold with a relatively high melting point was deposited on the prepared polymer mold via e-beam evaporation, thereby forming the metal nanostructure (see Figure 2a(6)). Subsequently, Ag films with different thicknesses were fabricated on the Si wafer with an ultra-thin Cr layer (see Figure 2a(7)). Here, a Cr layer with a thickness of 3 nm can strengthen the adhesion between AgNF and the Si wafer. Heterogeneous nanostructures were then obtained under a pressure of 6 bar, a heating time of 10 min, and heating temperatures from 120 to 200 °C (see Figure 2a(8,9)). Previous studies have reported a size-dependent melting temperature of noble metals at the nanoscale.[34,35] In addition, the atomic interdiffusion effects at the junctions of different noble metals under high temperatures have been evaluated in previous studies, resulting in the development of the nano-welding technique.[36,37] Based on these studies, we fabricated heterogeneous nanostructures using the proposed method. Notably, the morphologies can be controlled by adjusting the thickness of the metals, the heating temperature, and the size of the nanopatterns. Figure 2b demonstrates the large-area nanofabrication with a dimension of 100 mm × 100 mm without any defects observed via our method. Figure 2c shows the 3D image of the Ag nanoislands (AgNIs) located inside the Au nanoholes (AuNHs). The AgNF was completely melted during the heating process and reshaped as AgNIs owing to the boundary constraints of the AuNHs.

To observe the specific change in the fabricated nanostructures depending on different temperature conditions and sizes of the AuNHs, AuNHs with three different sizes (diameters: 200, 400, 750 nm) were exposed to various heating temperatures (120−200 °C). Figure 3a−c shows the morphology of the fabricated structures with three different sizes of AuNHs depending on the different heating temper-

https://dx.doi.org/10.1021/acsami.0c18122
ACS Appl. Mater. Interfaces 2021, 13, 3358−3368

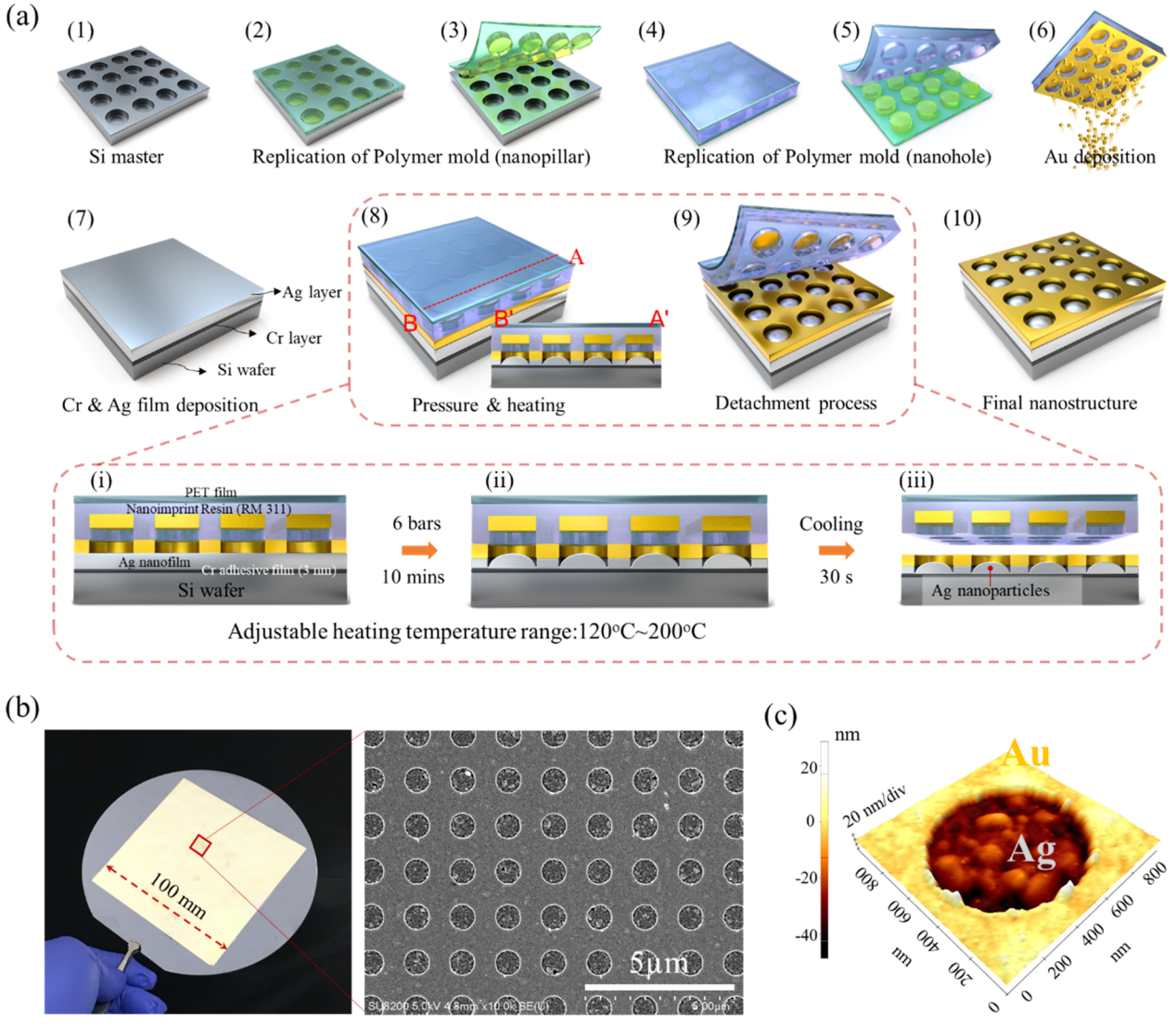

Figure 2. Fabrication process, large-area photo, and 3D image of heterogeneous nanostructures. (a) Nanofabrication process; (1−3) repeated replication process of the polymer mold with a nanopillar; (4, 5) replication of the polymer mold with a nanohole; (6) metal deposition; (7) preparation of Ag nanofilms; (8, 9) melting process (detail conditions (i−iii)); (10) final nanostructure. (b) Large-area fabrication with a dimension of 100 mm × 100 mm; the corresponding scanning electron microscopy (SEM) images are depicted on the right. (c) 3D images of heterogeneous nanostructures obtained by atomic force microscopy (AFM).

atures from 120 to 200 °C in increments of 20 °C (see i−v), as observed using a scanning electron microscope (SEM). AuNHs with a thickness of 15 nm were chosen for the fabrication of nanostructures owing to their relatively high melting point. The thickness of the Au metal can be adjusted according to the requirement of the nanofabrication process. From Figure 3a, it is observed that AgNPs located within AuNHs with a diameter of 200 nm gradually became smaller as the temperature increased from 120 to 200 °C, in increments of 20 °C (Figure 3a(i−v)). AuNHs did not show any observable changes when the heating temperature was varied, which was due to the relatively higher melting point of the Au metal compared to Ag. Conversely, when the heat was applied, the morphology of the AgNF appeared to change, owing to the lower melting point of the fabricated AgNF with a thickness of 10 nm (this phenomenon is consistent with the results of previous studies[33−36]). Figure 2a(i−v) illustrates the formation of AgNPs, which occurred as a result of temperature change, within the AuNHs (diameter = 200 nm). The AgNF was completely melted and reshaped as the isolated AgNPs under a heating temperature of over 140 °C. In addition, it was observed that AgNIs can be fabricated by increasing the size of the AuNHs. From Figure 3a−c, as the size of the outer AuNHs increased, the shape of the inner AgNF changed from that of AgNPs to AgNIs because of the larger size of the AgNF. From these results, it is clear that AgNIs and AgNPs can be well-arrayed and positioned inside the AuNHs. The SEM images (large-area) in Figure S1 clearly demonstrate the large-area nanofabrication of the nanostructures.

Three-dimensional (3D) images of these transformations are depicted in Figure 3d,e. In Figure 3d(1−3), the 3D morphologies of the heterogeneous nanostructures with AgNF of 10 nm (thickness) and AuNHs of 200 nm (diameter), as the temperature increased from 120 to 200 °C, in increments of 40 °C, are depicted. It can be observed that AgNPs are well aligned and positioned in the AuNHs. Furthermore, Figure 3e(1−3) depicts the 3D morphologies of AgNF of 10 nm (thickness) and AuNHs of 750 nm

https://dx.doi.org/10.1021/acsami.0c18122
ACS Appl. Mater. Interfaces 2021, 13, 3358−3368

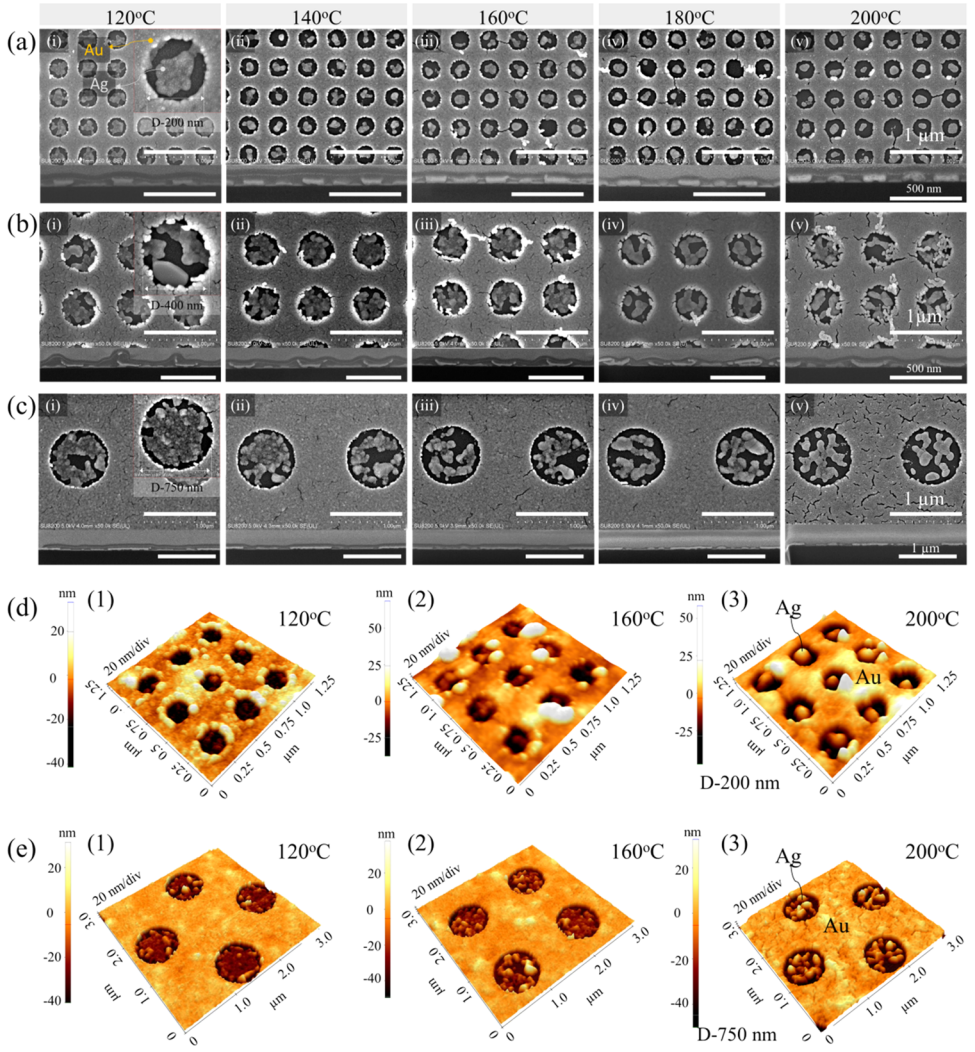

Figure 3. SEM, FIB-SEM, and AFM images of the fabricated heterogeneous nanostructures. (a−c) SEM morphologies depending on different heating temperatures ranging from 120 to 200 °C at intervals of 20 °C. (a) Heterogeneous nanostructures composed of AuNHs with a diameter of 200 nm and AgNF with a thickness of 10 nm; (b) AuNHs with a diameter of 400 nm and AgNF with a thickness of 10 nm; (c) AuNHs with a diameter of 750 nm and AgNF with a thickness of 10 nm (all scales are 1 μm). (d) and (e) AFM 3D images of different samples with AuNHs, with diameters of 200 and 750 nm depending on the different heating temperatures, ranging from 120 to 200 °C, at intervals of 40 °C.

(diameter), as the temperature increased from 120 to 200 °C, in increments of 40 °C. The transformation of AgNIs to AgNPs can be clearly observed. Therefore, the unique, simple, and economical nature of the proposed nanofabrication method makes it highly applicable in various fields, such as sensing, catalysis, plasmonics, and anti-counterfeiting.

Furthermore, for better evaluation and analysis of the compositions of the fabricated heterogeneous nanostructures, transmission electron microscopy (TEM), energy-dispersive spectroscopy (EDS)-mapping, and X-ray photoelectron spectroscopy (XPS) were used; the results thus obtained are presented in Figure 4. The cross-sectional images of the fabricated samples with AuNHs (diameter = 200 nm and thickness = 15 nm) and AgNF (thickness = 10 nm) are shown in Figure 4a(1−3). The compositions (Au, Ag, Cr, and native oxide) are marked in Figure 4a(3). Figure 4b(1−6) shows the EDS-mapping images, which demonstrate the clear composition of the heterogeneous nanostructures. The complete image is provided in Figure 4b(1), while Figure 4b(2−6) shows the individual elements (Si, O, Cr, Ag, and Au). To evaluate the state of the Au and Ag interface, the binding energy was measured using the etching method of XPS. Figure 4c shows the XPS spectrum of the heterogeneous nanostructure. Figure 4c(1) shows the relative atomic percentage of the composition of the fabricated samples based on the etching time. The binding energies for Au and Ag are shown in Figure 4c(2,3), and these values are based on the differences in their etching times. From these results, it can be conceded that no change in the binding energies of Au and Ag was observed. The morphology of the heterogeneous nanostructures can be controlled by changing the diameter of the AuNHs and adjusting the heating temperature depending on the requirement of the nanofabrication process. We also found that by altering the thickness of AgNF, the shape of the nanostructures can be effectively controlled. This is because the melting point of the metal increases with the thickness of the AgNF. To demonstrate the diverse nature of the AgNF located below the AuNHs (dependent on the thickness), AgNFs with thicknesses of 20, 30, and 40 nm were fabricated using the above-mentioned method. The specific changes in the morphology based on the different thicknesses of AgNF are illustrated in Figure S2.

https://dx.doi.org/10.1021/acsami.0c18122
ACS Appl. Mater. Interfaces 2021, 13, 3358−3368

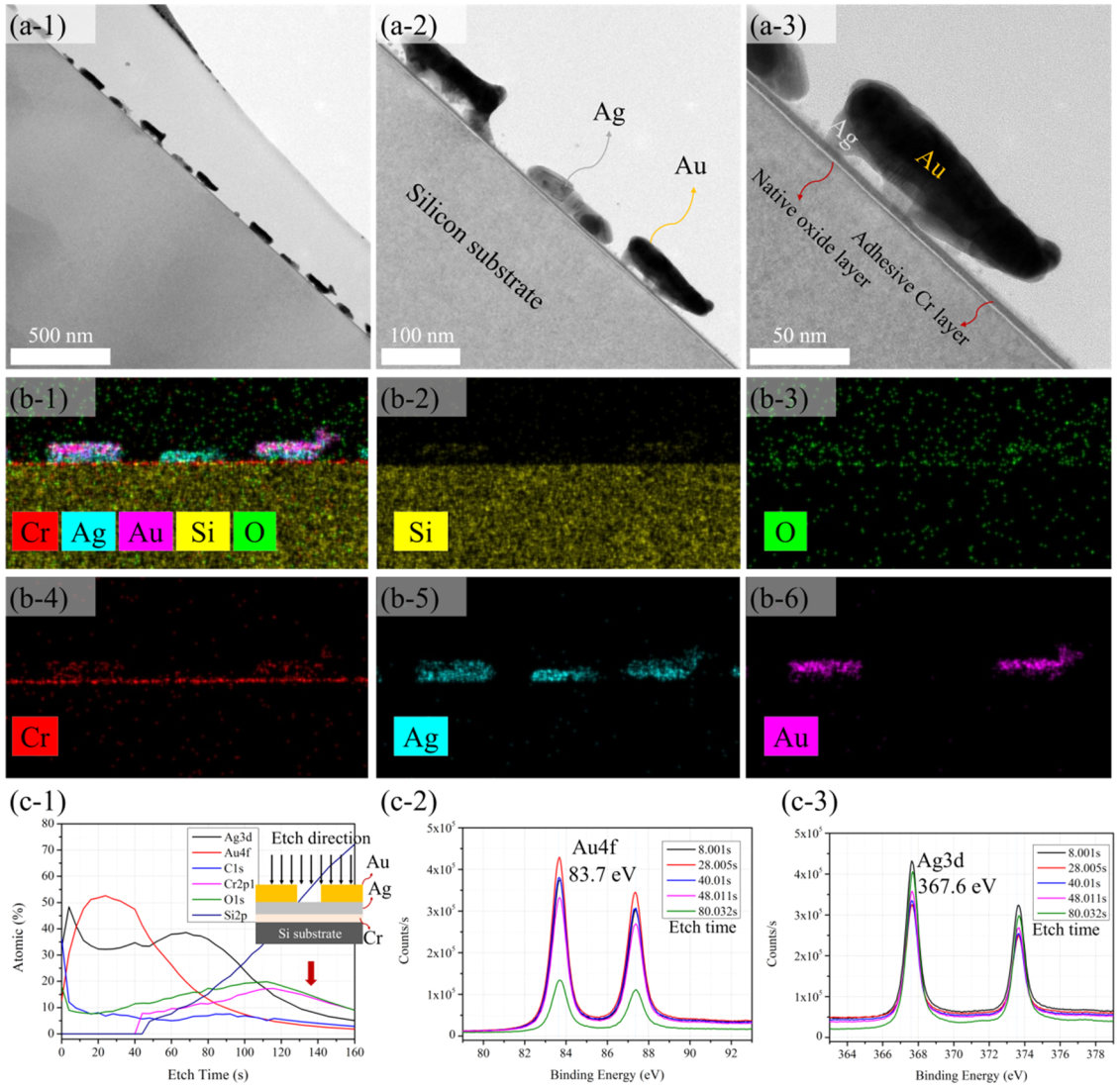

Figure 4. TEM images, EDS-mapping, and XPS analysis of the heterogeneous nanostructures. (a-1)−(a-3) TEM cross-sectional images; (b-1)−(b-6) EDS-mapping images (showing the distribution of chemical elements including Si, O, Cr, Ag, and Au). (c-1)−(c-3) Results of XPS analysis. (c-1)The relative atomic percentage of the element with the increase of etching time; (c-2) Au 4f; (c-3) Ag 3d.

The results of tests performed to further compare the changes in the morphology depending on the thickness of the AgNF are shown in Figure 5. Figure 5a,b(1−4) illustrates the morphologies of the heterogeneous nanostructures composed of AuNHs with a diameter of 200 nm and AgNF with different thicknesses of 10, 20, 30, and 40 nm, which were fabricated under heating temperatures, ranging from 120 to 200 °C. Figure 5c,d(1−4) illustrates the morphologies of the heterogeneous nanostructures composed of AuNHs with a diameter of 750 nm and AgNF with different thicknesses of 10, 20, 30, and 40 nm, which were fabricated under heating temperatures ranging from 120 to 200 °C. At a heating temperature of 120 °C, it is observed that the AgNF could not be heavily melted with an increase in the thickness; therefore, AgNPs could not be individually generated (Figure 5a(3,4)). However, the melted shape of the AgNF surfaces can be observed. Correspondingly, when the heating temperature was increased to 200 °C, AgNF melted from the center of the AuNHs along with an increase in the thickness (20−40 nm). This phenomenon is consistent with the findings presented in previous studies (size-dependent melting temperatures of noble metals at the nanoscale[34,35]). On the other hand, in Figure 5c,d(1−4), Ag nanogaps (AgNGs) are observed in AuNHs as the thickness and the size of AuNHs increased. The detailed images of the structures, as the temperature increased from 120 to 200 °C, are provided in Figure S2. In addition, the effects of heating time on the heterogeneous structure are shown in Figure S3.

Moreover, to demonstrate the uniformity aspect of our method, 16 points of the large fabricated area with a dimension of 100 mm × 100 mm were evaluated via SEM, as shown in Figure S4. Also, to investigate the reproducibility of the fabrication method, five different specimens were fabricated using the same fabrication conditions. The results show similar shapes of Ag nanostructures overall, although their details differ. The reason for this difference is that we can control the melting point and degree of melting by controlling the size of the Ag film, but the process of solidification after melting is relatively random, as shown in Figure S5. In addition, Figure S6 demonstrates the morphologies before and after the peel test using a 3M tape for confirming the stability of our method. From Figures S4−S6, we can conclude that our method

https://dx.doi.org/10.1021/acsami.0c18122
ACS Appl. Mater. Interfaces 2021, 13, 3358−3368

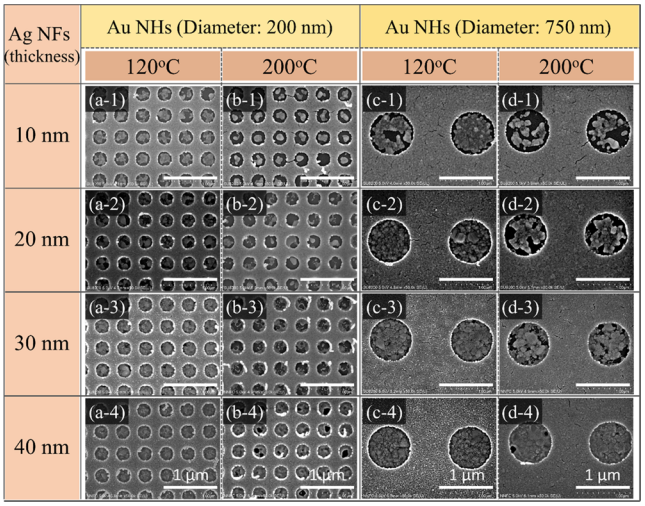

Figure 5. Diverse morphologies of the fabricated samples depending on the thicknesses of the AgNF ranging from 10 to 40 nm at intervals of 10 nm, the diameter of AuNHs (200, 750 nm), and the heating temperature (120, 200 °C). (a-1)−(a-4) Morphologies at a heating temperature of 120 °C and a AuNH diameter of 200 nm. (b-1)−(b-4) Heating temperature of 200 °C and a AuNH diameter of 200 nm. (c-1)−(c-4) Heating temperature of 120 °C and a AuNH diameter of 750 nm. (d-1)−(d-4) Heating temperature of 200 °C and a AuNH diameter of 750 nm.

provides particularly key advantages in terms of large-area production, uniformity, and mechanical stability for nanofabrication and its applications. In addition, our method is also suitable for the nanofabrication of various shapes depending on the requirement such as Au mesh type and wire type; corresponding images are provided in Figure S7 as a reference for future research.

To expand the applications of our method, various SERS substrates were fabricated based on different heating temperatures, diameters of AuNHs, and thicknesses of AgNFs. SERS analysis has been widely applied in the detection of small molecules because it provides extremely high sensitivity and specificity to the small molecules using the localized surface plasmon resonance effect of metal nanostructures.[38,39] In particular, when the target molecule is located inside the sub-10 nm nanogaps of the metal nanostructures, which are called the SERS hot spots, the Raman signal can be enhanced up to several orders of the original signal on the Si wafer substrate.[40] However, even though numerous studies dealing with the superior performance and design methods of the SERS substrates have been reported, it has not been widely commercialized because of critical limitations such as high-cost process, complex fabrication methods, and nonuniform performance.[42] Therefore, to overcome these limitations, the developed structures were utilized as a superior SERS substrate.

In the developed structure, the well-arrayed AuNHs facilitated evenly distributed hot spots at the boundary of AuNHs, and the AgNGs enhanced the Raman signal, as depicted in Figure 6a.[43] Figure 6b shows the Raman performance of the AgNIs, Au film, and Ag film. Although AgNPs exhibit a lower density of nanogaps compared with the AgNG structure, owing to their entirely reshaped Ag films, the Raman peaks of the R6G are clearly distinguished, while those of the film substrate are noisy. Figure 6c−e shows the effects of the heterogeneous nanostructures on the performance of the Raman signals according to the diameter of AuNHs, the heating temperature, and the thickness of AgNF, respectively. As the dimensions (thickness and diameter) of the Ag film inside the AuNHs increase, the Ag film forms a much higher density of nanogaps, as discussed. In addition, the extremely high heating temperature melts the Ag film completely, and the Ag film is reshaped as AgNIs or AgNPs. Therefore, the highest enhancement, which shows 1.06×10^6 times higher enhancement performance of the R6G Raman signal compared with that in the metal film, was achieved under the conditions of a AgNF thickness of 40 nm, a AuNH diameter of 750 nm, and a temperature of 120 °C. In addition, the developed well-arrayed heterogeneous nanostructures allowed uniform and reliable Raman signal detection. Figures 6f and S8 show the Raman signal of the nine different points on the same substrate. The average RSD is calculated as 19.8%, and it can be concluded that the developed structure is a promising, uniform, and reliable SERS substrate in comparison with the commercialized SERS substrates, which yield RSDs of 20−50%.[41] Therefore, the mass-producible, shape-controlled, and well-arrayed heterogeneous nanostructures with a high density of the AgNGs developed in this study can be effectively utilized as a novel SERS substrate.

The developed Ag−Au heterogeneous nanostructures were also used for nonreproducible anti-counterfeiting applications. As the total amount of counterfeiting worldwide is projected to reach 1.82 trillion USD by 2020, studies concerning the examination of anti-counterfeiting patterns have increased.[44] In addition, the development of reliable tagging techniques has become one of the most prominent research topics because increasing counterfeiting can not only cause direct economic loss but also affect defense security.[45] To prevent counterfeiting in an efficient manner, security patterns should meet the following conditions. (1) Structurally reliable/stable pattern: The patterns should be mechanically reliable and stable structures as they can be exposed to diverse harsh environments such as mechanical deformation, scratching, and humid/dry air. (2) Mass-producible pattern: For use in a wide range of real-life applications, these patterns need to be fabricated using a low-cost, simple, large-area process. (3) Nonreproducible but a markable pattern: To prevent counterfeiting, the patterns should not only be nonreproducible even with the same fabricating conditions but should also have specific regularity for proper marking and taggant readout. However, recently reported tagging techniques such as dendritic silver nanoparticles,[22] heterostructures,[23] luminescent magnetic nanoparticles,[46] and light-emitting ceramic nanopigments[47] do not satisfy the abovementioned conditions simultaneously owing to the complicated nature of fabrication procedures or their random structures. Therefore, fabrication of anti-counterfeiting signs with highly reliable, mass-producible, nonreproducible, and markable patterns continues to be a challenge.

As a solution to the aforementioned challenge, the fabricated AgNP and AgNI structures were utilized as anti-counterfeiting patterns. As shown in Figure 7a, these structures were fabricated on a PI film with a shadow mask, and a security code was assigned to each structure according to the number, average size, and fill ratio of the nanoparticles. Here, the tagging images were defined as an image appearing on one screen when enlarged 100 000 times (6 holes at diameter = 200 nm, 1 hole at diameter = 750 nm), the particle was defined as a black region surrounded by a white region, and the fill ratio was defined as the total particle area over the entire

https://dx.doi.org/10.1021/acsami.0c18122
ACS Appl. Mater. Interfaces 2021, 13, 3358−3368

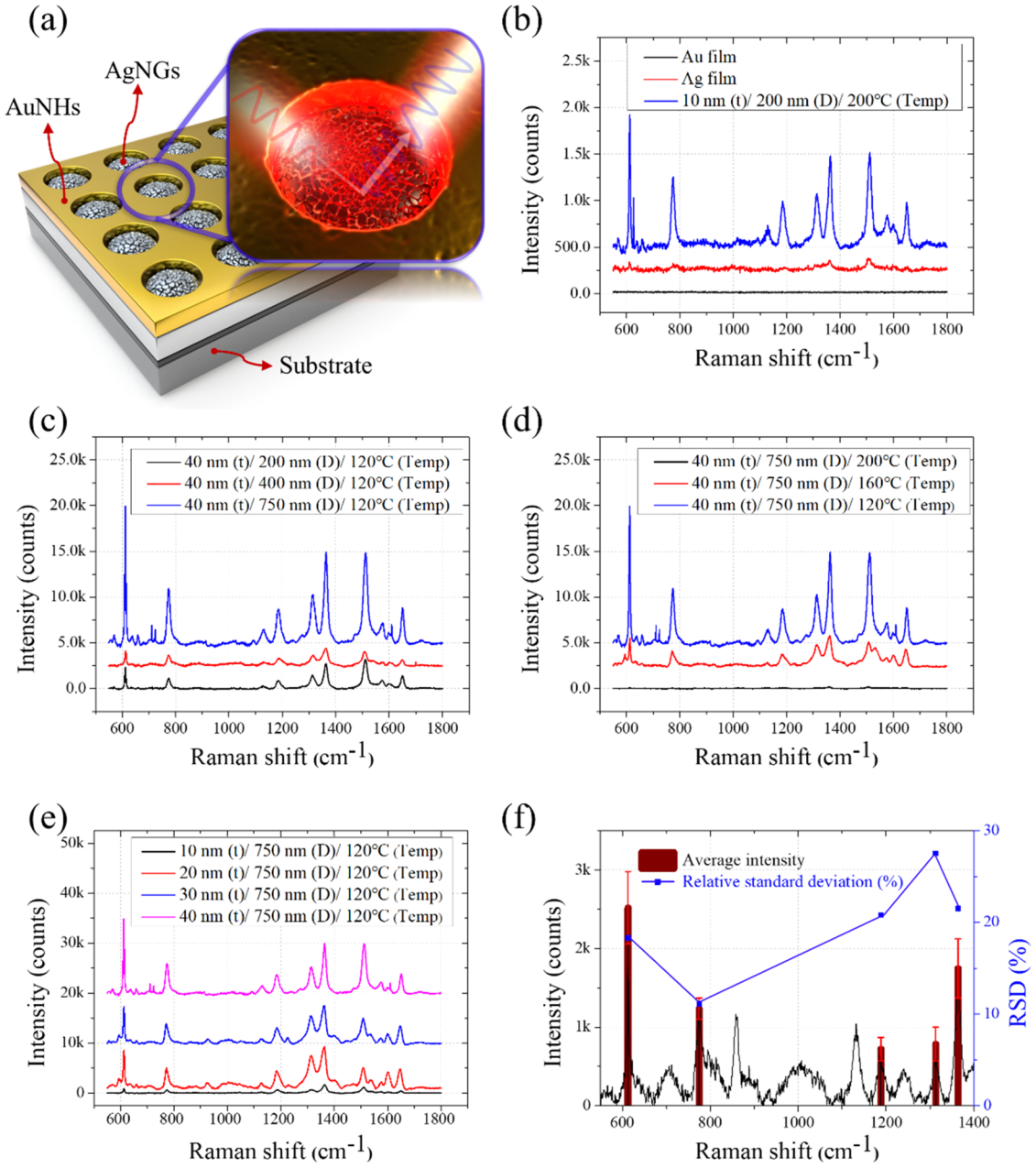

Figure 6. Performance and characterization of the heterogeneous nanostructures as a surface-enhanced Raman spectroscopy (SERS) substrate. (a) Schematic of the AgNGs-based SERS substrate with a high density of nanogaps. The red color on the enlarged view refers to the SERS hot spots between the nanogaps. (b) Comparison of the Raman enhancement effect between the AgNPs and the metal films. Enhancement performance of the Raman signal according to (c) the diameter of AuNHs, (d) heating temperature, and (e) thickness of the AgNF. (f) Uniformity tests of the SERS signal using nine different points on the same substrate. In this figure, "*t*" refers to the thickness of the AgNF, "*D*" refers to the diameter of the AuNHs, and "Temp" refers to the heating temperature.

tagging area. By scanning the security code and comparing it with the anti-counterfeiting patterns, which will be later attached to the objects, forgery can be easily checked. The macro-size numbering and horseshoe-shaped patterns were also used for marking the location of a specific security pattern, and this is expected to facilitate the verification process. In addition, the flexible, mechanically/chemically stable, and transparent substrate, which can be attached to any arbitrary shape including curved surfaces, will facilitate the practical use. Figure 7b shows SEM images of several AgNPs and AgNIs. For assigning a unique security code to each structure, the SEM images were converted into black/white images with an appropriate threshold and analyzed using image processing software, as shown in Figure 7c. It can also be observed that the image of (c-i) has a greater number of particles than that of (c-iii) but low area size and fill ratio. This is because the boundary AuNHs limited the size of AgNPs from the inside. In contrast, most of the AgNPs in the (c-ii) were connected to each other owing to a low heating temperature, which resulted in a small number of particles, low fill ratio, and small average size. As shown in Figure 7d,e, by controlling the heating temperatures, the diameter of AuNHs, and the thickness of AgNF, highly reliable and nonreproducible security patterns can be easily fabricated. In addition, the developed security

https://dx.doi.org/10.1021/acsami.0c18122
ACS Appl. Mater. Interfaces 2021, 13, 3358−3368

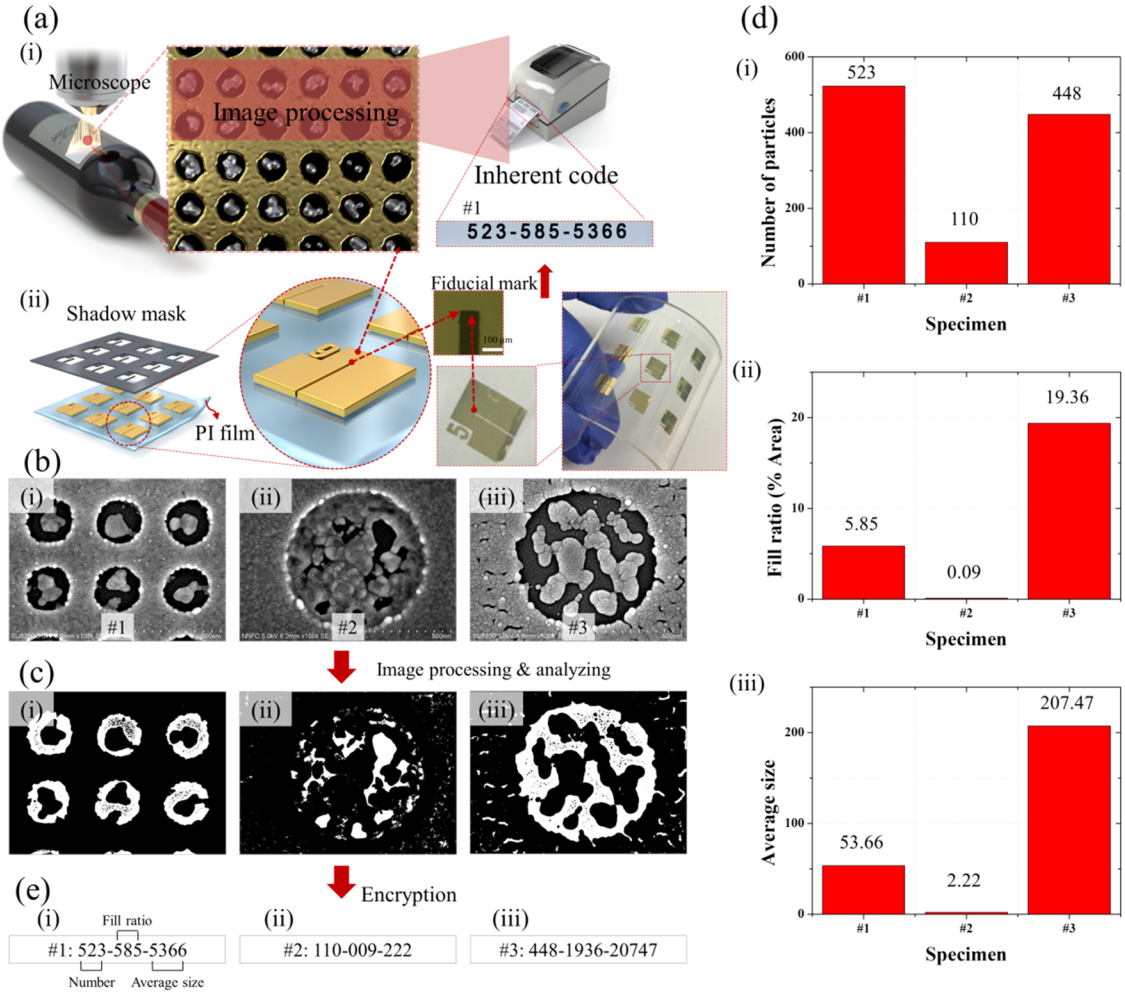

Figure 7. Application of the Ag−Au heterogeneous nanostructures as anti-counterfeiting signs. (a) Schematic of the anti-counterfeiting/readout system. Security codes were assigned to each image based on the number, average size, and fill ratio of AgNPs. The particle was defined as a black region surrounded by a white one. (b) SEM image of the AgNP and AgNI structures. (c) Black/white images converted from SEM images. (d) Results of image analysis according to the number of particles, fill ratio, and the average size. (e) A number was assigned to each image.

patterns can maintain their unique structures even after immersion in water or vibrating on a shaker for one week owing to their structural robustness, as shown in Figure S9. Therefore, we can conclude that the developed AgNP and AgNI structures can be effectively utilized as reliable/stable, mass-producible, nonreproducible, and markable anti-counterfeiting signs.

CONCLUSIONS

In this study, a novel method for fabricating shape-controlled and well-arrayed heterogeneous nanostructures by adjusting the melting point of metals at the nanoscale was developed. The AgNI, AgNP, and AgNG structures were successfully and orderly fabricated inside the AuNHs by modulating the diameter of AuNHs, the thickness of AgNF, and the heating temperature. The experimental results clearly demonstrated the diverse morphologies and cross-sectional images via SEM, FIB, atomic force microscopy (AFM), and TEM. With the proposed nanofabrication process, uniformity, mechanical stability, large-area production, and flexibility were also demonstrated. Finally, diverse practical applications of the developed nanostructures were demonstrated. Various SERS substrates that showed enhancement effects were compared and analyzed according to various conditions. The results showed that the AgNG sample fabricated using Ag NFs with a thickness of 40 nm and AuNHs with a diameter of 750 nm at 120 °C heating temperature showed a superior enhancement performance, which is 1.06×10^6 times higher than that of a metal film, with a reasonable RSD of 19.8%. In addition, based on the uniqueness of the proposed method, anti-counterfeit signs were designed to demonstrate the anti-counterfeiting/readout systems via image processing. These anti-counterfeiting patterns showed structurally reliable/stable, mass-producible, nonreproducible, and easily markable characteristics. In conclusion, the proposed method allows for the facile fabrication of shape-controlled and well-arrayed heterogeneous nanostructures, and practical applications such as use as a SERS substrate and anti-counterfeiting patterns were successfully demonstrated. Therefore, we believe that the present study provides a new research direction in the field of nanofabrication of functional heterogeneous nanostructures.

METHODS

The nanofabrication process employed in this study consists of ten (10) sequential steps, as shown in Figure 2a(1−10). The steps are discussed in detail below.

Silicon Master. Silicon (Si) master was prepared using KrF lithography. The Si master was then treated with a self-assembled

https://dx.doi.org/10.1021/acsami.0c18122
ACS Appl. Mater. Interfaces 2021, 13, 3358−3368

monolayer (SAM) to facilitate easier separation of the polymer from the mold.[48] Trichloro(1*H*,1*H*,2*H*,2*H*-perfluorooctyl)silane was selected as the SAM treatment material (Sigma-Aldrich).

Replication of Polymer Mold (Nanopillars). RM-311 resin (Minuta Technology Co., Ltd. Korea, polyurethane) was coated onto the surface of the prepared Si master (Figure 2a(2,3)). A transparent polyethylene (PET) film with a thickness of 100 μm as a substrate was covered on the resin. To facilitate the complete penetration of the resin onto the nanopatterns of the Si master, the pressure was applied using a hand roller. Ultraviolet (UV) light was then used to make the resin fully polymerized, thereby forming the polymer mold by separating from the Si master. This process can be repeatedly replicated using the Si master.

Replication of Polymer Mold (Nanoholes). To obtain the polymer mold with nanoholes, the second replication was implemented using the fabricated polymer mold as a template, thereby obtaining a polymer mold with nanoholes (Figure 2a(4,5)).

Gold (Au) Deposition. AuNHs with a thickness of 15 nm were deposited on the polymer mold with nanoholes under a vacuum of approximately 6×10^{-6} torr, at a rate of 1.0 Å/s using an e-beam evaporator (Figure 2a(6)).

Cr and Ag Deposition. The Cr thin film with a thickness of 3 nm was deposited as an adhesive layer on the Si substrate, and, then, AgNF with different thicknesses (10−40 nm) were fabricated on the Cr layer (Figure 2a(7)).

Pressure, Heating, and Detachment Process. The fabricated AuNHs were placed on the AgNF under a pressure of 6 bar. The sample was heated for 10 min at 120 °C. Subsequently, it was cooled for 1 min, following which the AuNHs were transferred onto AgNF, owing to the stronger adhesion of the Cr layer. The morphologies of the heterogeneous nanostructures could be controlled by adjusting the heating temperature, the thickness of AgNF, and the diameter of AuNHs (Figure 2a(8,9)).

Fabricated Nanostructures. The morphology of the AgNF in the as-obtained heteronomous nanostructures changed from film-island to particles when the heating temperature was adjusted (Figure 2a(10)).

Characterization. Ultra-high-resolution field-emission SEM (UHR FE-SEM; SU8230, Hitachi high-technologies Corp., Japan) and FIB (Helios, FEI, Netherlands) were used to evaluate the morphologies and cross-sections of the fabricated samples. High-resolution transmission electron microscopy (HRTEM) (JEM-ARM200FM, JEOL, Japan) was performed to observe the junction of the layers of the fabricated nanostructures. Simultaneously, EDS-mapping was used to confirm the position of different metals. XPS (K-α+, Thermo Fisher Scientific, Inc.) was performed to analyze the binding energy of the two metals. Additionally, AFM (XE-100, Park Systems) was used to analyze the specific changes in the shapes of the AgNF at different heating temperatures. Dispersive Raman Spectrometry (ARAMIS, Horiba Jobin Yvon, France) with a 633 nm laser was used to measure the SERS signal.

SERS Measurement of the R6G Solution. For SERS detection, Rhodamine 6G (56226, Sigma Aldrich) was coated on the heterogeneous nanostructures. A solution of 27 μL of Rhodamine 6G with a concentration of 10^{-6} M for the heterogeneous nanostructures and another with a concentration of 10^{-3} M for the metal film were poured on 1 cm^2 substrates, followed by solvent drying. Next, the SERS signals were measured using a dispersive Raman spectrometer (ARAMIS, Horiba Jobin Yvon, France) with a 633 nm laser. Raman signals were collected for 5 s. For the evaluation of the RSD, representative Rhodamine6G peaks, such as 612, 774, 1183, 1310, and 1363 nm, were used.

Imaging Processing Method. The processing of SEM images of the heterogeneous nanostructures was conducted using the freely available ImageJ program (National Institutes of Health and the Laboratory for Optical and Computational Instrumentation, University of Wisconsin). Security codes were assigned to each image based on the number, average size, and fill ratio of the AgNPs. The particle was defined as a black region surrounded by a white region. To fabricate a flexible anti-counterfeit film, the abovementioned process was applied to the PI film.

■ ASSOCIATED CONTENT

Supporting Information

The Supporting Information is available free of charge at https://pubs.acs.org/doi/10.1021/acsami.0c18122.

Low-magnification SEM images of the fabricated samples (Figure S1); SEM morphologies of the fabricated heterogeneous nanostructures depending on the heating temperature (120−200 °C) (Figure S2); the morphologies of heterogeneous nanostructures depending on the heating time from 1 to 20 min at an interval of 2 min (Figure S3); low- and high-magnification SEM images of the heterogeneous nanostructures fabricated on the 6 in. wafer (Figure S4); SEM images of the five different specimens fabricated using the same conditions (Figure S5); low- and high-magnification SEM images of the heterogeneous nanostructures before and after peel test (Figure S6); SEM images of the fabricated well-aligned nanostructures with various shapes (Figure S7); Raman signal of the R6G molecule on the nine different points of the same substrate (Figure S8); results of long-term stability test for anti-counterfeiting applications (Figure S9) (PDF)

■ AUTHOR INFORMATION

Corresponding Authors

Inkyu Park − *Department of Mechanical Engineering, Korea Advanced Institute of Science and Technology (KAIST), Daejeon 34141, South Korea;* orcid.org/0000-0001-5761-7739; Email: inkyu@kaist.ac.kr

Jun-Ho Jeong − *Nano-Convergence Mechanical Systems Research Division, Korea Institute of Machinery and Materials, Daejeon 34103, South Korea; Department of Nano Mechatronics, University of Science and Technology (UST), Daejeon 34103, South Korea;* orcid.org/0000-0003-0671-0225; Email: jhjeong@kimm.re.kr

Authors

Zhi-Jun Zhao − *Nano-Convergence Mechanical Systems Research Division, Korea Institute of Machinery and Materials, Daejeon 34103, South Korea*

Junseong Ahn − *Nano-Convergence Mechanical Systems Research Division, Korea Institute of Machinery and Materials, Daejeon 34103, South Korea; Department of Mechanical Engineering, Korea Advanced Institute of Science and Technology (KAIST), Daejeon 34141, South Korea*

Jiwoo Ko − *Nano-Convergence Mechanical Systems Research Division, Korea Institute of Machinery and Materials, Daejeon 34103, South Korea; Department of Mechanical Engineering, Korea Advanced Institute of Science and Technology (KAIST), Daejeon 34141, South Korea*

Yongrok Jeong − *Nano-Convergence Mechanical Systems Research Division, Korea Institute of Machinery and Materials, Daejeon 34103, South Korea*

Moonjeong Bok − *Nano-Convergence Mechanical Systems Research Division, Korea Institute of Machinery and Materials, Daejeon 34103, South Korea*

Soon Hyoung Hwang − *Nano-Convergence Mechanical Systems Research Division, Korea Institute of Machinery and Materials, Daejeon 34103, South Korea*

https://dx.doi.org/10.1021/acsami.0c18122
ACS Appl. Mater. Interfaces 2021, 13, 3358−3368

Hyeok-Joong Kang − *Nano-Convergence Mechanical Systems Research Division, Korea Institute of Machinery and Materials, Daejeon 34103, South Korea*
Sohee Jeon − *Nano-Convergence Mechanical Systems Research Division, Korea Institute of Machinery and Materials, Daejeon 34103, South Korea*
Jungrak Choi − *Department of Mechanical Engineering, Korea Advanced Institute of Science and Technology (KAIST), Daejeon 34141, South Korea*

Complete contact information is available at: https://pubs.acs.org/10.1021/acsami.0c18122

Author Contributions

Z.-J.Z. and J.A. contributed equally. Z.-J.Z. and J.A. performed all experiments, analyzed the data, and wrote the manuscript. Z.-J.Z, J.A., and J.K. fabricated and characterized the 3D nanocomposite architectures. Y.J., M.B., S.H.H., H.-J.K, S.J., and J.C. discussed the results. I.P. and J.-H.J. led the overall direction of the project. All authors have given their approval to the final version of the manuscript.

Funding

This work was supported by the Center for Advanced Meta-Materials (CAMM) funded by the Ministry of Science, ICT, and Future Planning, Korea, through the Global Frontier Project (CAMM-No. 2014M3A6B3063707), Institute of Information & Communications Technology Planning & Evaluation (IITP) grant funded by the Korea government (MSIT)(No. 2020-0-00831, Development of holographic lithography equipment and printing technology for security and books) and the Basic Research Program of KIMM (Korea Institute of Machinery and Materials, NK224C). This work was also supported by the National Research Foundation of Korea (NRF) grant funded by the Korea government (MSIT) (No. 2018R1A2B2004910).

Notes

The authors declare no competing financial interest.

■ ABBREVIATIONS USED

AgNF, silver nanofilm
AgNI, silver nanoisland
AgNP, silver nanoparticle
AuNH, gold nanohole
SERS, surface-enhanced Raman spectroscopy
AFM, atomic force microscopy
SEM, scanning electron microscopy
FIB, focused ion beam
R6G, rhodamine6G
XPS, X-ray photoelectron spectroscopy
TEM, transmission electron spectroscopy

■ REFERENCES

(1) Guo, S.; Yu, P.; Li, W.; Yi, Y.; Wu, F.; Mao, L. Electron Hopping by Interfacing Semiconducting Graphdiyne Nanosheets and Redox Molecules for Selective Electrocatalysis. *J. Am. Chem. Soc.* **2020**, *142*, 2074−2082.
(2) Ma, H.; Zheng, W.; Yan, X.; Li, S.; Zhang, K.; Liu, G.; Jiang, L. Polydopamine-induced fabrication of Ag-TiO2 hollow nanospheres and their application in visible-light photocatalysis. *Colloids Surf., A* **2020**, *586*, No. 124283.
(3) Khanum, R.; Das, N. M.; Moirangthem, R. S. Defect Engineered ZnO Whispering Gallery Modes Via Doping With Alkali Metal Ions For Label-Free Optical Sensors. *J. Appl. Phys.* **2019**, *125*, No. 173107.
(4) Kumari, S.; Moirangthem, R. S. Portable and Economical Plasmonic Capillary Sensor for Biomolecular Detection. *Sens. Actuators, B* **2016**, *231*, 203−210.
(5) Aslan, K.; Wu, M.; Lakowicz, J. R.; Geddes, C. D. Fluorescent Core−Shell Ag@ SiO2 Nanocomposites for Metal-enhanced Fluorescence and Single Nanoparticle Sensing Platforms. *J. Am. Chem. Soc.* **2007**, *129*, 1524−1525.
(6) Li, X.; Kwon, H.-j.; Qi, X.; Choi, H. K.; Lim, S.; Kim, T.-W.; Kim, S. H. Direct-patterned Copper/Poly (Ethylene Oxide) Composite Electrodes for Organic Thin-Film Transistors Through Cone-Jet Mode by Electrohydrodynamic Jet Printing. *J. Ind. Eng. Chem.* **2020**, *85*, 269−275.
(7) Wen, R.; Guo, J.; Yu, A.; Zhai, J.; Wang, Z. L. Humidity-Resistive Triboelectric Nanogenerator Fabricated Using Metal Organic Framework Composite. *Adv. Funct. Mater.* **2019**, *29*, No. 1807655.
(8) Eperon, G. E.; Hörantner, M. T.; Snaith, H. J. Metal Halide Perovskite Tandem and Multiple-Junction Photovoltaics. *Nat. Rev. Chem.* **2017**, *1*, No. 0095.
(9) Kundu, D.; Adams, B. D.; Duffort, V.; Vajargah, S. H.; Nazar, L. F. A High-Capacity and Long-Life Aqueous Rechargeable Zinc Battery Using a Metal Oxide Intercalation Cathode. *Nat. Energy* **2016**, *1*, No. 16119.
(10) Arbabi, A.; Arbabi, E.; Horie, Y.; Kamali, S. M.; Faraon, A. Planar Metasurface Retroreflector. *Nat. Photonics* **2017**, *11*, 415−420.
(11) Zhao, Z.-J.; Hwang, S. H.; Kang, H.-J.; Jeon, S.; Bok, M.; Ahn, S.; Im, D.; Hahn, J.; Kim, H.; Jeong, J.-H. Adhesive-Layer-Free and Double-Faced Nanotransfer Lithography for a Flexible Large-Area MetaSurface Hologram. *ACS Appl. Mater. Interfaces* **2020**, *12*, 1737−1745.
(12) Baek, S. W.; Park, G.; Noh, J.; Cho, C.; Lee, C. H.; Seo, M. K.; Song, H.; Lee, J. Y. Au@ Ag Core−Shell Nanocubes for Efficient Plasmonic Light Scattering Effect in Low Bandgap Organic Solar Cells. *ACS Nano* **2014**, *8*, 3302−3312.
(13) Zhao, Z. J.; Lee, M.; Kang, H.; Hwang, S.; Jeon, S.; Park, N.; Park, S. H.; Jeong, J. H. Eight Inch Wafer-Scale Flexible Polarization-Dependent Color Filters with Ag−TiO2 Composite Nanowires. *ACS Appl. Mater. Interfaces* **2018**, *10*, 9188−9196.
(14) Cao, G.; Wang, Y. *Nanostructures and Nanomaterials: Synthesis, Properties, and Applications*; World Scientific, 2011, Vol. *2*.
(15) Roduner, E. Size Matters: Why Nanomaterials are Different. *Chem. Soc. Rev.* **2006**, *35*, 583−592.
(16) Wang, M.; Feng, Y. Palladium−Silver Thin Film for Hydrogen Sensing. *Sens. Actuators, B* **2007**, *123*, 101−106.
(17) Wadell, C.; Nugroho, F. A. A.; Lidström, E.; Iandolo, B.; Wagner, J. B.; Langhammer, C. Hysteresis-Free Nanoplasmonic Pd−Au Alloy Hydrogen Sensors. *Nano Lett.* **2015**, *15*, 3563−3570.
(18) Zhao, Z. J.; Ko, J.; Ahn, J.; Bok, M.; Gao, M.; Hwang, S. H.; Kang, H. J.; Jeon, S.; Park, I.; Jeong, J. H. 3D Layer-by-Layer Pd-Containing Nanocomposite Platform for Enhancing Performance of Hydrogen Sensor. *ACS Sens.* **2020**, *5*, 2367−2377.
(19) Baibarac, M.; Cochet, M.; Łapkowski, M.; Mihut, L.; Lefrant, S.; Baltog, I. SERS Spectra of Polyaniline Thin Films Deposited on Rough Ag, Au and Cu. Polymer Film Thickness and Roughness Parameter Dependence of SERS Spectra. *Synth. Met.* **1998**, *96*, 63−70.
(20) Yang, Y.; Shi, J.; Kawamura, G.; Nogami, M. Preparation of Au−Ag, Ag−Au Core−Shell Bimetallic Nanoparticles for Surface-enhanced Raman Scattering. *Scr. Mater.* **2008**, *58*, 862−865.
(21) Qin, X.; Si, Y.; Wang, D.; Wu, Z.; Li, J.; Yin, Y. Nanoconjugates of Ag/Au/Carbon Nanotube for Alkyne-meditated Ratiometric SERS Imaging of Hypoxia in Hepatic Ischemia. *Anal. Chem.* **2019**, *91*, 4529−4536.
(22) Zhao, Z.; Chamele, N.; Kozicki, M.; Yao, Y.; Wang, C. Photochemical Synthesis of Dendritic Silver Nano-Particles for Anti-counterfeiting. *J. Mater. Chem. C* **2019**, *7*, 6099−6104.
(23) Yang, C.; Gu, L.; Ma, C.; Gu, M.; Xie, X.; Shi, H.; Ma, H.; Yao, W.; An, Z.; Huang, W. Controllable Co-Assembly of Organic Micro/Nano Heterostructures from Fluorescent and Phosphorescent

Molecules for Dual Anti-counterfeiting. *Mater. Horiz.* **2019**, *6*, 984−989.
(24) Shankar, S. S.; Rai, A.; Ahmad, A.; Sastry, M. Rapid synthesis of Au, Ag, and Bimetallic Au Core−Ag shell Nanoparticles Using Neem (*Azadirachta indica*) Leaf Broth. *J. Colloid Interface Sci.* **2004**, *275*, 496−502.
(25) Olea-Mejía, O.; Fernández-Mondragón, M.; Rodríguez-de la Concha, G.; Camacho-López, M. SERS-Active Ag, Au and Ag−Au Alloy Nanoparticles Obtained by Laser Ablation in Liquids for Sensing Methylene Blue. *Appl. Surf. Sci.* **2015**, *348*, 66−70.
(26) Innocenzi, P.; Malfatti, L. Mesoporous Materials as Platforms for Surface-enhanced Raman Scattering. *TrAC, Trends Anal. Chem.* **2019**, *114*, 233−241.
(27) Sun, Y.; Jiang, L.; Zhong, L.; Jiang, Y.; Chen, X. Towards Active Plasmonic Response Devices. *Nano Res.* **2015**, *8*, 406−417.
(28) Yang, Y.; Zhang, Z.; He, Y.; Wang, Z.; Zhao, Y.; Sun, L. Fabrication of Ag@ TiO2 Electrospinning Nanofibrous Felts As SERS Substrate for Direct and Sensitive Bacterial Detection. *Sens. Actuators, B* **2018**, *273*, 600−609.
(29) Sánchez-Iglesias, A.; Carbó-Argibay, E.; Glaria, A.; Rodríguez-González, B.; Pérez-Juste, J.; Pastoriza-Santos, I.; Liz-Marzán, L. M. Rapid Epitaxial Growth of Ag on Au Nanoparticles: From Au Nanorods to Core−Shell Au@ Ag Octahedrons. *Chem. - Eur. J.* **2010**, *16*, 5558−5563.
(30) Wang, R.; Xu, Y.; Wang, R.; Wang, C.; Zhao, H.; Zheng, X.; Liao, X.; Cheng, L. A Microfluidic Chip Based on an ITO Support Modified With Ag-Au Nanocomposites for SERS Based Determination of Melamine. *Microchim. Acta* **2017**, *184*, 279−287.
(31) Sivashanmugan, K.; Lee, H.; Syu, C.-H.; Liu, B. H.-C.; Liao, J.-D. Nanoplasmonic Au/Ag/Au Nanorod Arrays As SERS-Active Substrate for the Detection of Pesticides Residue. *J. Taiwan Inst. Chem. Eng.* **2017**, *75*, 287−291.
(32) Yuan, X. Synthesis and Characterization of New Au-Ag Plasmonic Alloy Materials. M.Sc. Thesis, Science: Department of Chemistry, 2019.
(33) Wu, Y.; Akiyama, T.; Gautsch, S.; de Rooij, N. Development of Passivated Heterogeneous Metal Nanogaps Using E-Beam Overlay Techniques. *Procedia Eng.* **2011**, *25*, 1661−1664.
(34) Jiang, Q.; Zhang, S.; Zhao, M. Size-Dependent Melting Point of Noble Metals. *Mater. Chem. Phys.* **2003**, *82*, 225−227.
(35) Berman, R. P.; Curzon, A. E. The Size Dependence of the Melting Point of Small Particles of Indium. *Can. J. Phys.* **1974**, *52*, 923−929.
(36) Zhao, Z. J.; Shin, S. H.; Choi, D. G.; Park, S. H.; Jeong, J. H. Shape-controlled 3D Periodic Metal Nanostructures Fabricated Via Nanowelding. *Small* **2018**, *14*, No. 1703102.
(37) Zhao, Z. J.; Hwang, S.; Bok, M.; Kang, H.; Jeon, S.; Park, S. H.; Jeong, J. H. Nanopattern-embedded Micropillar Structures for Security Identification. *ACS Appl. Mater. Interfaces* **2019**, *11*, 30401−30410.
(38) Kelley, S. O.; Mirkin, C. A.; Walt, D. R.; Ismagilov, R. F.; Toner, M.; Sargent, E. H. Advancing the Speed, Sensitivity and Accuracy of Biomolecular Detection Using Multi-Length-Scale Engineering. *Nat. Nanotechnol.* **2014**, *9*, 969−980.
(39) Kosaka, P. M.; Pini, V.; Ruz, J. J.; Da Silva, R. A.; González, M. U.; Ramos, D.; Calleja, M.; Tamayo, J. Detection of Cancer Biomarkers in Serum Using a Hybrid Mechanical and Optoplasmonic Nanosensor. *Nat. Nanotechnol.* **2014**, *9*, 1047−1053.
(40) Jeong, J. W.; Arnob, M. M. P.; Baek, K.-M.; Lee, S. Y.; Shih, W.-C.; Jung, Y. S. 3D Cross-Point Plasmonic Nanoarchitectures Containing Dense and Regular Hot Spots for Surface-Enhanced Raman Spectroscopy Analysis. *Adv. Mater.* **2016**, *28*, 8695−8704.
(41) Thai, T.; Zheng, Y.; Ng, S. H.; Mudie, S.; Altissimo, M.; Bach, U. Self-Assembly of Vertically Aligned Gold Nanorod Arrays on Patterned Substrates. *Angew. Chem., Int. Ed.* **2012**, *51*, 8732−8735.
(42) Yang, S.; Cai, W.; Kong, L.; Lei, Y. Surface Nanometer-Scale Patterning in Realizing Large-Scale Ordered Arrays of Metallic Nanoshells with Well-defined Structures and Controllable Properties. *Adv. Funct. Mater.* **2010**, *20*, 2527−2533.
(43) Lee, T.; Wi, J. S.; Oh, A.; Na, H. K.; Lee, J.; Lee, K.; Lee, T. G.; Haam, S. Highly Robust, Uniform and Ultra-Sensitive Surface-Enhanced Raman Scattering Substrates for microRNA Detection Fabricated by Using Silver Nanostructures Grown in Gold Nanobowls. *Nanoscale* **2018**, *10*, 3680−3687.
(44) Global Brand Counterfeiting Report. https://www.researchandmarkets.com/research/7j7l2n/global_brand?w=4, 2018.
(45) Senate Armed Services Committee Releases Report on Counterfeit Electronic Parts. https://www.armed-services.senate.gov/press-releases/senate-armed-services-committee-releases-report-on-counterfeit-electronic-parts.
(46) Li, C.; Hai, J.; Li, S.; Wang, B.; Yang, Z. Luminescent Magnetic Nanoparticles Encapsulated in MOFs for Highly Selective and Sensitive Detection of Clo−/SCN− and Anti-Counterfeiting. *Nanoscale* **2018**, *10*, 8667−8676.
(47) Darshan, G. P.; Premkumar, H. B.; Nagabhushana, H.; Sharma, S. C.; Prashantha, S. C.; Nagaswarup, H. P.; Prasad, B. D. Blue Light Emitting Ceramic Nano-Pigments of Tm3+ Doped YAlO3: Applications in Latent Finger Print, Anti-counterfeiting and Porcelain Stoneware. *Dyes Pigm.* **2016**, *131*, 268−281.
(48) Zhao, Z. J.; Hwang, S. H.; Jeon, S.; Jung, J. Y.; Lee, J.; Choi, D. G.; Choi, J. H.; Park, S. H.; Jeong, J. H. Effects of Polymer Surface Energy on Morphology and Properties of Silver Nanowire Fabricated Via Nanoimprint and E-Beam Evaporation. *Appl. Surf. Sci.* **2017**, *420*, 429−438.

https://dx.doi.org/10.1021/acsami.0c18122
ACS Appl. Mater. Interfaces 2021, 13, 3358−3368